THE JOURNAL OF BIOLOGICAL CHEMISTRY VOL. 289, NO. 31, pp. 21519–21532, August 1, 2014

Altered Inhibition of Cx26 Hemichannels by pH and Zn^{2+} in the A40V Mutation Associated with Keratitis-Ichthyosis-Deafness Syndrome*

Received for publication, May 2, 2014, and in revised form, June 4, 2014 Published, JBC Papers in Press, June 17, 2014, DOI 10.1074/jbc.M114.578757

Helmuth A. Sanchez[‡], **Rick Bienkowski**[§], **Nefeli Slavi**[¶], **Miduturu Srinivas**[¶], **and Vytas K. Verselis**[‡1]

From the [‡]*Dominick P. Purpura Department of Neuroscience, Albert Einstein College of Medicine, Bronx, New York 10461, the* [§]*Department of Cell Biology, Emory University School of Medicine, Atlanta, Georgia 30322, and the* [¶]*Department of Biological Sciences, SUNY College of Optometry, New York, New York 10036*

Background: Aberrantly functioning Cx26 hemichannels are a common feature of *GJB2* mutations causing syndromic deafness.
Results: pH and Zn^{2+}, factors that inhibit hemichannels, are less effective in the A40V KID syndrome mutant.
Conclusion: Impaired inhibition by pH and Zn^{2+} can contribute to the pathogenesis of KID syndrome.
Significance: Data provide new insights into Cx26 hemichannel function and possible contributions to tissue function.

Excessive opening of undocked Cx26 hemichannels in the plasma membrane is associated with disease pathogenesis in keratitis-ichthyosis-deafness (KID) syndrome. Thus far, excessive opening of KID mutant hemichannels has been attributed, almost solely, to aberrant inhibition by extracellular Ca^{2+}. This study presents two new possible contributing factors, pH and Zn^{2+}. Plasma pH levels and micromolar concentrations of Zn^{2+} inhibit WT Cx26 hemichannels. However, A40V KID mutant hemichannels show substantially reduced inhibition by these factors. Using excised patches, acidification was shown to be effective from either side of the membrane, suggesting a protonation site accessible to H^+ flux through the pore. Sensitivity to pH was not dependent on extracellular aminosulfonate pH buffers. Single channel recordings showed that acidification did not affect unitary conductance or block the hemichannel but rather promoted gating to the closed state with transitions characteristic of the intrinsic loop gating mechanism. Examination of two nearby KID mutants in the E1 domain, G45E and D50N, showed no changes in modulation by pH or Zn^{2+}. *N*-bromo-succinimide, but not thiol-specific reagents, attenuated both pH and Zn^{2+} responses. Individually mutating each of the five His residues in WT Cx26 did not reveal a key His residue that conferred sensitivity to pH or Zn^{2+}. From these data and the crystal structure of Cx26 that suggests that Ala-40 contributes to an intrasubunit hydrophobic core, the principal effect of the A40V mutation is probably a perturbation in structure that affects loop gating, thereby affecting multiple factors that act to close Cx26 hemichannels via this gating mechanism.

Mutations in the *GJB2* gene that codes for the connexin 26 (Cx26) gap junction (GJ)[2] protein result in non-syndromic and syndromic forms of sensorineural deafness. Connexins are the substrates of GJ channels, which are specialized intercellular channels that serve to communicate electrical and chemical signals directly between cells. Hexamers of connexin subunits inserted in the plasma membrane form hemichannels that dock across the extracellular space between neighboring cells to form a complete GJ channel. However, hemichannels can function in the plasma membrane in the absence of docking, thereby conferring both intercellular and transmembrane signaling roles to connexins.

Cx26 mutations that result in non-syndromic deafness generally produce loss of function as a result of deletions, frameshifts, and truncations. However, syndromes such as keratitis-ichthyosis-deafness (KID) and palmoplantar keratoderma are associated with missense mutations that typically produce functional hemichannels that exhibit aberrant properties (1–3). Thus, association of skin disorders with deafness appears to be a gain of function attributable to hemichannels. Recently, a transgenic mouse developed by Mese *et al.* (4) that expressed the Cx26 KID syndrome mutation G45E in keratinocytes remarkably reproduced the skin phenotype observed in human patients. Increased hemichannel activity also was recorded in keratinocytes that matched the properties observed in exogenous expression systems (5). Furthermore, several studies have reported that hemichannels act as conduits for the release of ATP and inositol 1,4,5-triphosphate from cochlear support cells (6–8).

The aberrant hemichannel properties of KID mutants generally have been described by the term "leaky" to denote increased activity in the plasma membrane (1, 9). Connexin hemichannels have a large pore diameter, and increased activity can compromise cell integrity through loss of cytoplasmic solutes and

* This work was supported, in whole or in part, by National Institutes of Health Grants GM054179 (to V. K. V.), EY013869 (to M. S.), and T32 NS007439 (to H. A. S).

[1] To whom correspondence should be addressed: Dept. of Neuroscience, Albert Einstein College of Medicine, 1300 Morris Park Ave., Bronx, NY 10461. Tel.: 718-430-3680; Fax: 718-430-8944; E-mail: vytas.verselis@einstein.yu.edu.

[2] The abbreviations used are: GJ, gap junction; KID, keratitis-ichthyosis-deafness; TM1 and TM2, first and second transmembrane domain, respectively; E1, first extracellular loop domain; MTS, methane thiosulfonate; MTSET, 2-trimethylammonioethylmethane thiosulfonate; MTSES, 2-sulfonatoethylmethane thiosulfonate; NBS, *N*-bromosuccinimide; DEPC, diethylpyrocarbonate; BCECF, 2′,7′-bis-(2-carboxyethyl)-5-(and-6)-carboxyfluorescein; BCECF-AM, acetoxymethyl ester of BCECF; CT, carboxyl terminus; CL, cytoplasmic loop.

entry of extracellular ions. For the most part, the "leaky" phenotype has been ascribed to impaired regulation by extracellular Ca^{2+} (5, 9–14). Ca^{2+} is a robust inhibitor of connexin hemichannels, including Cx26.

Previously, we examined three KID syndrome mutations, A40V, G45E, and D50N, which are all are positioned near the border of the first transmembrane (TM1) and first extracellular loop (E1) domains (5, 14). Although each of these mutant hemichannels exhibits impaired inhibition by Ca^{2+}, there is a poor correlation between the degree of impaired inhibition and the severity of the disease phenotype. Thus, additional aberrant hemichannel properties are probably contributing to tissue dysfunction. In support, we demonstrated that two of these three mutations, G45E and D50N, occur at pore-lining residues, which can contribute to disease by altering permeability, as suggested by the enhanced permeability to Ca^{2+} for G45E hemichannels (5, 14). Here we continued to investigate other potential aberrant hemichannel properties. pH has been shown to regulate connexin hemichannels (15–17), and we examined whether sensitivity to pH in KID mutant Cx26 hemichannels was altered in a way that could contribute to increased hemichannel opening. We confirmed the robust sensitivity of human Cx26 hemichannels to changes in bath pH previously reported (17) and found that A40V hemichannels were substantially impaired in their ability to close with acidification. Interestingly, accompanying reduced inhibition by pH was reduced inhibition by Zn^{2+}. Among the three KID mutants studied here, impaired inhibition by pH and Zn^{2+} was specific to A40V. Previously, we showed that Ala-40 is not pore-lining (5), and the Cx26 crystal structure suggests that this residue participates in a hydrophobic core that stabilizes subunit structure (18). We discuss possible structure-function implications and underlying mechanisms of hemichannel inhibition by pH and Zn^{2+}.

MATERIALS AND METHODS

Construction of Cx26 Mutants—Human wild-type Cx26 was cloned into the BamHI restriction site of the $pCS2^{+}$ expression vector for functional studies in *Xenopus laevis* oocytes. A40V, G45E, D50N, and His mutants were prepared as described previously (5, 10). All site-directed mutations were constructed using the QuikChange mutagenesis kit (Stratagene, La Jolla, CA) in accordance with the manufacturer's protocol using the WT connexin expression constructs as templates. All constructs were verified by sequencing.

Exogenous Expression of Connexins—For expression of connexins in *Xenopus* oocytes, RNA was synthesized, and oocytes were prepared and injected as described previously (19, 20). Injected oocytes were maintained at 16–18 °C in a modified ND96 solution (MND96) containing 100 mM NaCl, 2 mM KCl, 1 mM $MgCl_2$, 1.8 mM $CaCl_2$, 10 mM glucose, 10 mM HEPES, 5 mM pyruvate, pH adjusted to 7.6. Recordings were done at room temperature.

Reagents—The methane thiosulfonate (MTS) reagents, 2-trimethylammonioethylmethane thiosulfonate (MTSET) and 2-sulfonatoethylmethane thiosulfonate (MTSES) were purchased from Anatrace (Maumee, OH). 2-(6-Biotinoylamino-hexanoyl-aminoethyl methanethiosulfonate was purchased from Biotium (Hayward, CA). Aliquots of dry powder were prepared and stored in microcentrifuge tubes at −20 °C. Prior to each experiment, aliquots of MTSET and MTSES were dissolved in distilled water, chilled on ice, to stock concentrations of 200 mM. Dilutions were made into appropriate perfusion solutions just prior to application to a final concentration of 0.2 mM for MTSET and 2 mM for MTSES. 2-(6-Biotinoylamino-hexanoyl-aminoethyl methanethiosulfonate was dissolved in DMSO to a stock concentration of 200 mM and diluted to a concentration of 0.2 mM. Diethylpyrocarbonate (DEPC) and *N*-bromosuccinimide (NBS) were purchased from Sigma, and fresh stocks were prepared for each experiment. DEPC was diluted to a stock concentration of 50 mM and diluted to a final concentration of 0.2 mM in recording solution. NBS was stored in aliquots of dry powder and was dissolved to a stock concentration of 2.5 mM and diluted to a concentration of 0.25 mM.

Macroscopic Electrophysiological Recording—Macroscopic hemichannel currents in *Xenopus* oocytes were recorded as described previously (5). Briefly, oocytes were placed in a polycarbonate RC-1Z recording chamber (Warner Instruments, Hamden, CT) with inflow and outflow compartments. The outflow compartment contained agar bridges connected to a VG-2A virtual ground bath clamp (Molecular Devices, Sunnyvale CA). All recordings were obtained with a GeneClamp 500 two-electrode voltage clamp (Molecular Devices, Sunnyvale CA). Both current-passing and voltage-recording pipettes contained 1 M KCl. During recording, oocytes were perfused with simple salt solutions that contained 100 mM NaCl, 1 mM $MgCl_2$, and 10 mM HEPES to which $CaCl_2$ was added to adjust Ca^{2+} concentration to desired levels. When testing the effects of buffers, HEPES was replaced with Tris or sodium bicarbonate. In HEPES- or Tris-buffered solutions, pH was adjusted with HCl and NaOH. For sodium bicarbonate solutions, pH was typically alkaline, and pH was adjusted by bubbling with 5% CO_2 until pH reached the desired level. This was done just prior to use in experiments. A check of the pH of the sodium bicarbonate solutions after each experiment showed no appreciable change in pH.

Monitoring Changes in Intracellular pH—Xenopus oocytes were loaded with the pH indicator 2′,7′-bis-(2-carboxyethyl)-5-(and-6)-carboxyfluorescein (BCECF) by exposing them for 60 min to 10 μM BCECF-AM (Invitrogen), the membrane-permeant acetoxymethyl ester of BCECF. The dye was alternately excited using wavelengths of 440 and 490 nm, and emission fluorescence was monitored at 540 nm using a Hamamatsu cooled digital camera and UltraVIEW software (PerkinElmer Life Sciences). We performed calibrations in NMD96 solutions in which NaCl was replaced with KCl using the acid form of BCECF at a concentration of 10 μM. Calibration solutions ranged from pH 5.5 to 8.0. Although this calibration does not provide a strict quantitative measure of intracellular pH in *Xenopus* oocytes, our intention was simply to assess whether there were large differences in relative changes in pH in oocytes exposed to solutions buffered with HEPES or sodium bicarbonate.

Single Hemichannel Recording—For patch clamp recordings of single hemichannel currents, *Xenopus* oocytes were manually devitellinized in a hypertonic solution consisting of 220 mM sodium aspartate, 10 KCl, 2 $MgCl_2$, 10 HEPES and then placed in the MND96 solution for recovery. Oocytes were then individually moved to a recording cham-

ber (RC-28, Warner Instruments Corp.) containing patch pipette solution (IPS), which consisted of 140 mM KCl, 1 mM $MgCl_2$, 0.5 mM $CaCl_2$, 3 mM BAPTA (1,2-bis(*o*-aminophenoxy)ethane-*N,N,N′,N′*-tetraacetic acid), and either 5 mM HEPES or 5 mM Tris; pH was adjusted to desired levels with KOH. The bath compartment was connected via a 3 M agar bridge to a ground compartment containing the same IPS solution. Single hemichannel *I*-V curves were obtained by applying 8-s voltage ramps from −70 to +70 mV. Currents were leak-subtracted by measuring leak conductance of a given patch during full closing transitions and extrapolating linearly over the entire voltage range. Currents were typically filtered at 1 kHz, and data were acquired at 5 kHz.

Acquisition of Electrophysiological Data—In electrophysiological experiments using oocytes, data were acquired with AT-MIO-16X D/A boards from National Instruments (Austin, TX) using custom acquisition software (written by E. B. Trexler, Gotham Scientific, Hasbrouck Heights, NJ).

RESULTS

Effects of pH on WT Cx26 and Mutant Hemichannels Associated with KID Syndrome—Hemichannel currents for WT Cx26 and three KID syndrome mutants, A40V, G45E, and D50N, were recorded in HEPES-buffered bath solutions adjusted to pH 8.0 and pH 6.5 (Fig. 1*A*). These three mutations are clustered in the proximal segment of E1, near the TM1/E1 border. Both G45E and D50N currents, like those of WT Cx26, decreased substantially upon reducing the bath from pH 8.0 to pH 6.5. In contrast, A40V currents were notably less affected by bath acidification. Ratios of the macroscopic conductances at pH 6.5 and 8.0 (G(pH 6.5)/G(pH 8.0)) are shown in Fig. 1*B*. Inhibition of hemichannels by pH was robust for G45E and D50N, similar to WT Cx26, but was substantially impaired for A40V. Inhibition by extracellular Ca^{2+}, calculated as the ratio of conductances in 0.2 and 2.0 mM Ca^{2+}, shows a different pattern for the three mutants (Fig. 1*C*). A40V exhibited modestly impaired inhibition by Ca^{2+} and, to a greater extent, pH. D50N exhibited a near loss of inhibition by Ca^{2+} (14) but maintained substantial inhibition by pH. G45E hemichannels maintained robust inhibition by pH and Ca^{2+}. Thus, these KID syndrome mutations differentially affect Ca^{2+}- and pH-mediated hemichannel regulatory mechanisms.

Sensitivity to pH Is Shifted in A40V Hemichannels—WT Cx26 hemichannel currents decreased progressively with bath pH below 8.0 with substantial inhibition evident at typical plasma pH levels of ~7.4 (Fig. 2*A*). A40V hemichannels showed attenuated responses to bath acidification over the same pH range. The responses also generally appeared slower, although this was not quantified. Plots of the fraction of current remaining at each pH relative to that at pH 8.0 (I/I(pH 8.0)) over a pH range from 6.5 to 8.0 show that WT Cx26 hemichannel currents declined to 50% of the maximum at a pH of ~7.2–7.3 (Fig. 2*B*). A40V hemichannel currents declined by ~20% in this pH range, and at a pH of 6.5, they declined by ~60% in comparison with the nearly complete inhibition of WT Cx26 currents. Thus, A40V hemichannels remain responsive to bath pH but with sensitivity shifted such that considerably more hemichannels remain open at plasma pH levels. Hemichannel currents recorded in oocytes exposed to pH values lower than 6.5 often recovered poorly upon returning to pH 8.0 and were not examined further.

pH Inhibition of Cx26 Hemichannels Expressed in Xenopus Oocytes Is Not Sensitive to pH Buffers—Studies of Cx26-containing hemichannels purified from rodent tissues and reconstituted into liposomes reported that the protonated forms of aminosulfonate pH buffers, such as HEPES, accounted for the apparent pH sensitivity of the liposome-reconstituted channels (21, 22). Studies of the action of taurine, a biological amimosulfonate, in cultured mammalian cells expressing Cx26 suggested a mechanism by which aminosulfonates disrupt a pH-dependent association between two intracellular domains, the carboxyl terminus (CT) and the cytoplasmic loop (CL), leading to occlusion of the pore (23). Thus, we examined whether pH responses of WT Cx26 and A40V hemichannels differed with and without an aminosulfonate buffer present in the bath by comparing pH responses in HEPES, Tris, and sodium bicarbonate; the latter two are not aminosulfonates. In the case of Tris, oocytes were placed in a Tris-buffered MND96 solution immediately after harvesting and were not exposed to HEPES. pH in bicarbonate-buffered solutions could not be stably maintained without a constant atmosphere of CO_2, and thus oocytes were kept in HEPES or Tris and then perfused with sodium bicarbonate adjusted to the desired pH with CO_2 just prior to experimentation. For WT Cx26, perfusion with solutions acidified to pH 7.1 produced robust responses in all three buffers; for sodium bicarbonate buffer, responses were the same if oocytes were previously maintained in HEPES or Tris (Fig. 3*A*). A40V responses to pH were weaker but similar in all buffers.

Although inhibition by pH in all buffers was similar, the use of sodium bicarbonate and CO_2 to lower pH should differ by producing a stronger and more rapid intracellular acidification due to the high membrane permeability of CO_2 and subsequent conversion to H^+ and HCO_3^- in the cytoplasm. To compare changes in intracellular pH in oocytes exposed to acidified solutions bathed in HEPES *versus* sodium bicarbonate, we used the fluorescent pH indicator BCECF. The low pH solutions were adjusted to 6.8, and exposure was limited to 2–3 min, a time sufficient to achieve nearly steady-state reductions in hemichannel currents. In the examples shown, oocytes expressing WT Cx26 or A40V (Fig. 3*B*) hemichannels showed little or no measureable changes in BCECF fluorescence when switching between HEPES-buffered solutions at pH 8.0 and pH 6.8. Upon subsequently switching to a sodium bicarbonate-buffered solution, exposure to pH 6.8 produced a rapid and substantial change in BCECF fluorescence. Although intracellular pH was not strictly quantified, the changes in fluorescence ratios measured in sodium bicarbonate solutions suggested a drop in bulk intracellular pH in the 6.4 – 6.6 range (see "Materials and Methods"). Recordings of hemichannel currents from these same oocytes show that WT and A40V hemichannels responded to pH in both buffers (Fig. 3*C*), indicating that sensitivity to pH is not dependent on the buffer or on bulk cytoplasmic acidification.

pH Is Effective from Extracellular and Intracellular Sides of Cx26 Hemichannels—Although our results, thus far, establish that acidification of the bath produces robust hemichannel

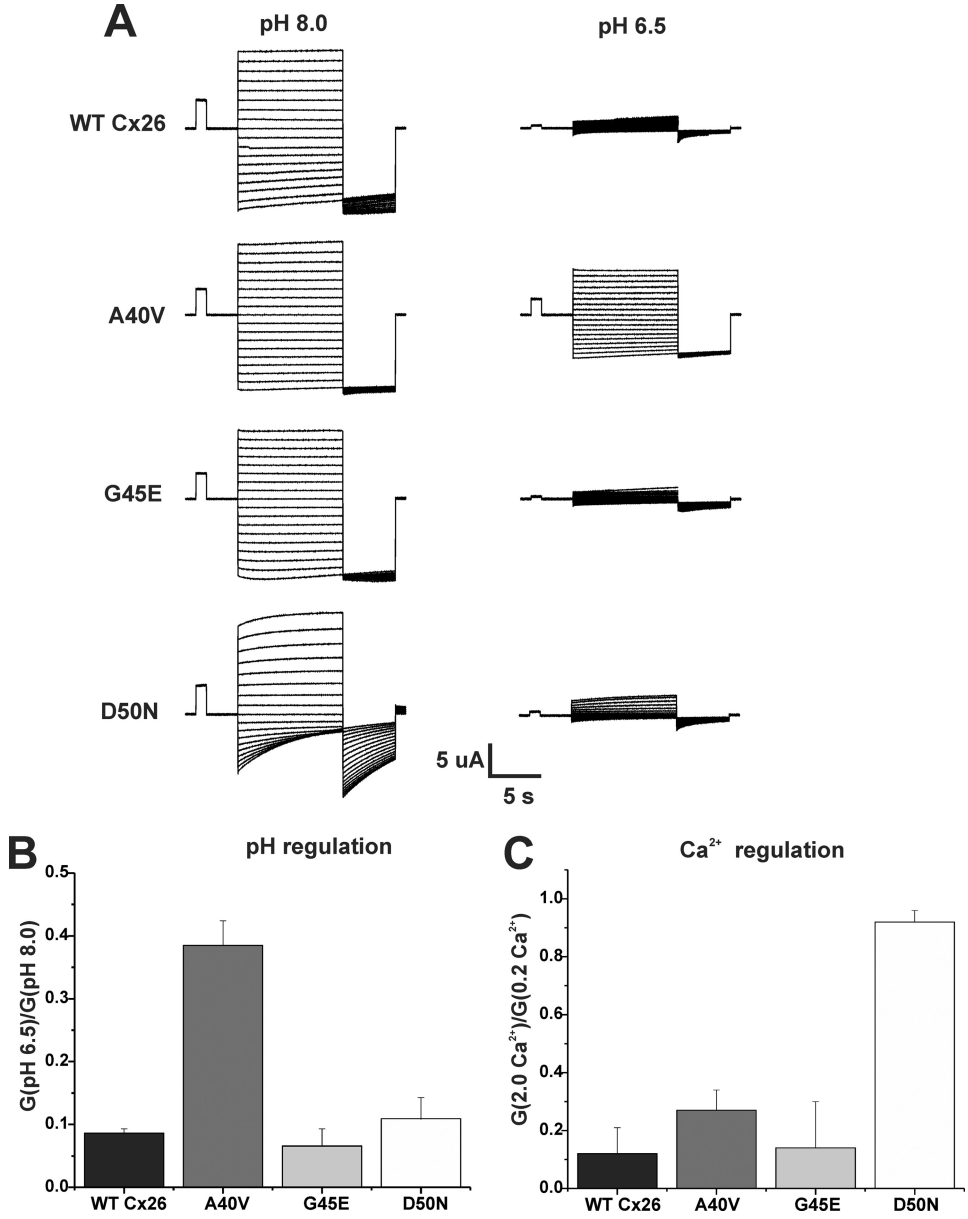

FIGURE 1. **A40V hemichannels exhibit an altered response to pH.** *A*, representative WT Cx26, A40V, G45E, and D50N hemichannel currents recorded in HEPES-buffered bath solutions adjusted to pH 8.0 and pH 6.5. Ca^{2+} was maintained at 0.2 mM. To obtain the families of hemichannel currents shown, oocytes were voltage-clamped to −20 mV, from which a voltage step protocol was applied that consisted of 10-s steps, ranging from +60 to −100 mV, in intervals of 10 mV followed by a 5-s step to −110 mV. *B*, bar graph showing ratios of macroscopic conductances in pH 6.5 and pH 8.0 (*G*(pH 6.5)/*G*(pH 8.0)). Conductances were calculated from currents elicited by brief (500-ms) voltage steps of ±10 and ±20 mV applied from a holding potential of −20 mV. The calculated conductances were averaged for the ±10- and ±20-mV voltage steps; no voltage dependence was evident during these small, brief steps. Each *bar* represents the mean ratio ± S.E. (*error bars*). $n = 5$ for WT Cx26, 5 for A40V, 5 for G45E, and 5 for D50N. *C*, bar graph showing responses to extracellular Ca^{2+} depicted as the ratios of macroscopic conductances in 2.0 and 0.2 mM Ca^{2+} ($G(2.0\ Ca^{2+})/G(0.2\ Ca^{2+})$). Ratios were obtained from currents elicited in response to small, brief voltage steps as described for pH in *B*. Each *bar* represents the mean ratio ± S.E. $n = 12$ for WT Cx26, 8 for A40V, 12 for G45E, and 10 for D50N.

inhibition, we wanted to verify that inhibition still occurred when only a patch of membrane was exposed to low pH. It is possible that sensitivity to pH resides on the cytoplasmic side, and whole-bath acidification produces rapid acidification at the inner membrane surface in the local vicinity of the hemichannel due to bulk flow across the membrane. Conversely, H^+ supplied from a small patch would diffuse rapidly away from the source and result in reduced or absent pH sensitivity. Thus, we compared WT Cx26 hemichannel recordings in cell-attached patches using high pH (8.0) and low pH (6.5) solutions in the patch pipettes. Comparisons were made in the same oocytes using multiple recordings that alternated between pH 8.0 and pH 6.5 in the pipette. Examples of recordings using pH 8.0 and pH 6.5 in the pipette are shown in Fig. 4*A*. The positive pressure applied to the back of the pipette was released in the bath prior to contacting the oocyte and establishing a high-resistance seal to gently mix the pH at the pipette tip with that in the bath pH. This procedure produced a transiently higher pH at the pipette tip when using the acidified pipette solution and allowed better visualization of the effects of low pH. When the pH of the pipette was 8.0, the same as the bath, current in the patch generally remained high throughout the recording.

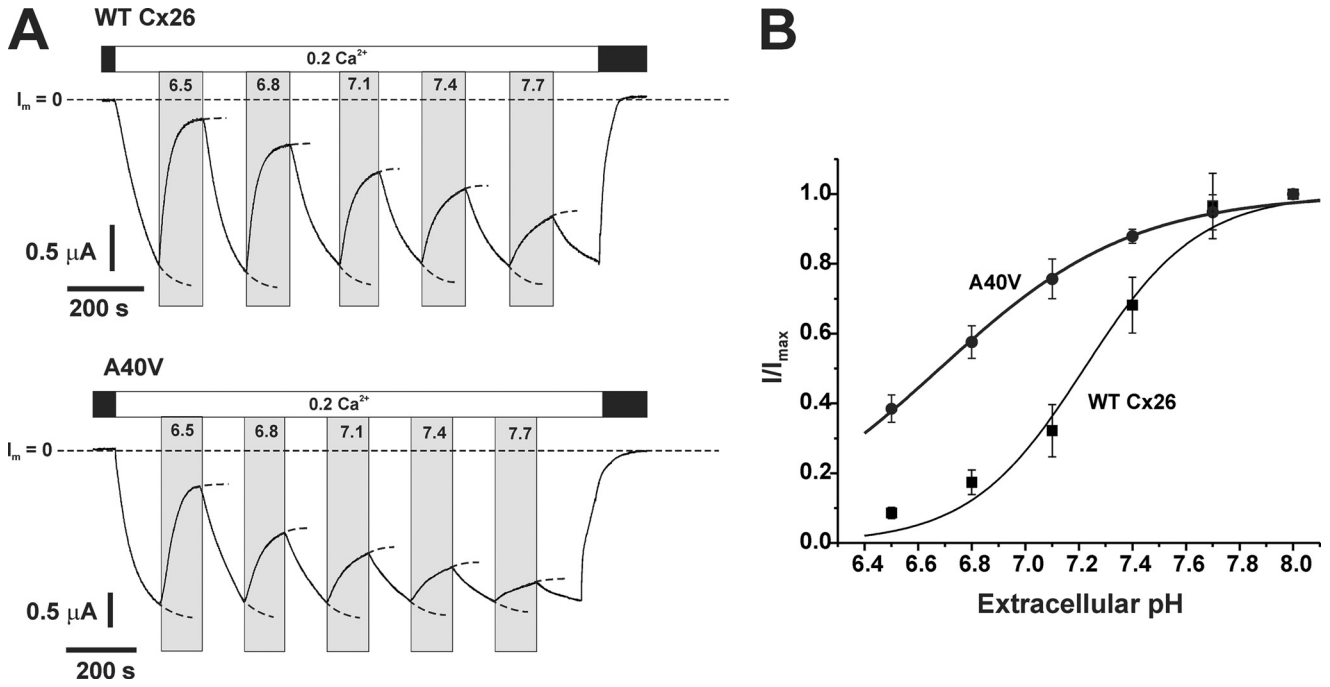

FIGURE 2. **The pH response curve is shifted in A40V hemichannels.** *A*, representative recordings of Cx26 WT and A40V hemichannel currents exposed to a series of bath solutions differing in pH. For each series, oocytes were initially placed in MND96 containing 1.8 mM Ca^{2+} (*black bars*) and then sequentially perfused with 100 mM NaCl solutions containing 0.2 mM Ca^{2+} and 10 mM HEPES adjusted to different pH values starting with pH 8.0. Between each exposure to an acidified pH solution, oocytes were returned to pH 8.0. Oocytes were returned to MND96 at the end of the experiment. Throughout, the oocytes were voltage-clamped and maintained at a constant voltage of −40 mV. *Dashed horizontal lines*, zero membrane current ($I = 0$). Responses to changes in pH were extrapolated to steady state by fits of the data to single exponential functions (illustrated by *dashed extrapolations* of currents). *B*, summary of average pH responses obtained from a series of sequential pH exposures as shown in *A*. Data are plotted as the fraction of steady-state current remaining relative to pH 8.0, I/I(pH 8.0). $n = 5$ oocytes for WT Cx26 and A40V. *Error bars*, S.D.

When the pH of the pipette was 6.5, currents were initially high, but they rapidly declined thereafter. Ensemble currents from seven patch recordings at each of the two pH values taken from the same oocyte showed substantially reduced currents when the pH in the patch pipette was low (Fig. 4*A*). There was some rundown in the current at pH 8.0 as well, but it did not account for the rapid decrease in current with low pH in the pipette.

Thus far, our results indicate that H^+ acts either extracellularly or at a site in or near the pore that is accessed by rapid flux through the hemichannel pore. To address the issue of sidedness of the pH effect, acidified solutions were applied to the cytoplasmic side of WT Cx26 hemichannels in excised patches. Fig. 4*B* shows an example of a recording in an inside-out patch configuration. Multiple hemichannels were active in the patch at pH 8.0, and perfusion of a pH 6.5 solution elicited rapid and robust closure. Upon returning to pH 8.0, the hemichannels reopened. Typically, recovery after acidification was partial, which may reflect rundown of hemichannel activity. However, as in the cell-attached patches, the rundown did not account for the rapid decrease in current with low pH applied to the bath. Moreover, the same results occurred with patches excised into solutions buffered with Tris.

pH Does Not Affect Unitary Conductance and Induces Closure Characteristic of Loop Gating—Comparison of single Cx26 hemichannel currents in cell-attached patches using pipettes with high and low pH exhibited no difference in unitary conductance. Shown in Fig. 5*A* are superimposed single hemichannel recordings obtained from separate patches, one at pH 8.0 and the other at pH 6.5. Currents are in response to voltage ramps (±70 mV). Although the hemichannel at pH 6.5 tended to reside more in a closed state, open hemichannel currents were of the same magnitude over the entire voltage range.

Examination of the closing events at low pH showed full closures with transitions that were indistinguishable from the loop gating transitions that typify voltage gating at hyperpolarized potentials. Loop gating transitions are characterized by multiple, transient substates en route to closure, giving the appearance that the transitions are slow when filtered (19). A recording from a cell-attached patch using a pipette filled with IPS at pH 6.5 (Fig. 5*B*) shows closures quickly induced after establishing a seal and stepping the voltage (*arrow*). An example of a typical pH-induced closing transition (*asterisk*) is shown in an *expanded view* and has these same characteristics as loop gating. We saw no evidence of additional types of rapid or flickery closing events that would signify channel block or a novel mechanism. These results suggest that the effect of pH on Cx26 hemichannels is local and leads to hemichannel closure via the loop gating mechanism.

A40V Hemichannels also Show Reduced Sensitivity to Extracellular Zn^{2+}—Considering that His and Cys residues, which contain titratable side chains near the neutral pH range, are good candidates to mediate the pH sensitivity of Cx26 hemichannels, we examined whether there was a concomitant change in A40V hemichannel sensitivity to metals such as Zn^{2+} that typically coordinate with His and Cys residues. WT Cx26 hemichannels show robust inhibition, with 1 μM Zn^{2+} producing ~70% inhibition (Fig. 6). G45E and D50N hemichannels showed a similar sensitivity to Zn^{2+} as WT Cx26. However, A40V

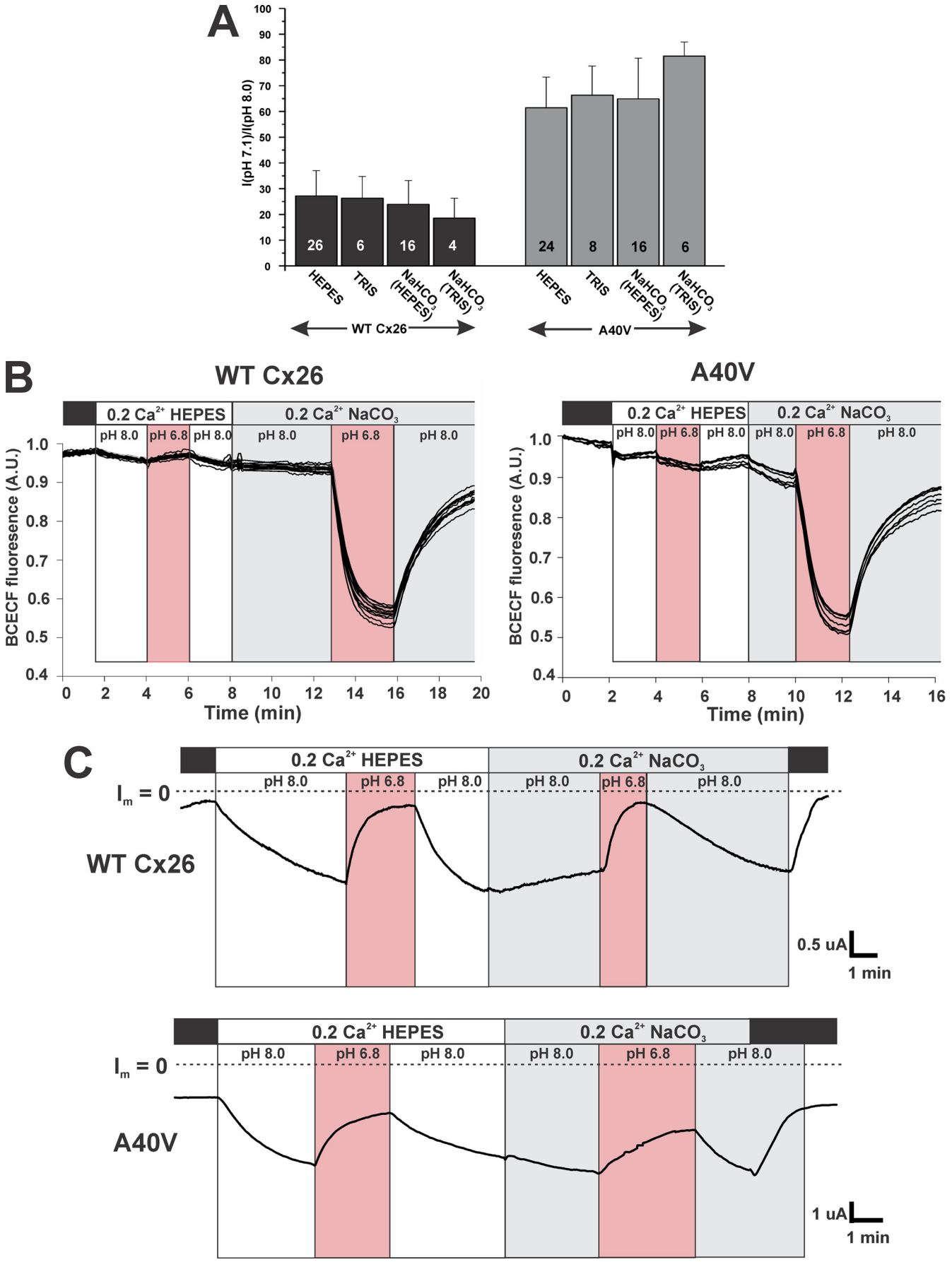
A
I(pH 7.1)/I(pH 8.0)
26
6
16
4
24
8
16
6
HEPES
TRIS
NaHCO3 (HEPES)
NaHCO3 (TRIS)
WT Cx26
A40V
B
WT Cx26
A40V
0.2 Ca2+ HEPES
0.2 Ca2+ NaCO3
pH 8.0
pH 6.8
BCECF fluoresence (A.U.)
Time (min)
C
Im = 0
WT Cx26
A40V
0.5 uA
1 uA
1 min

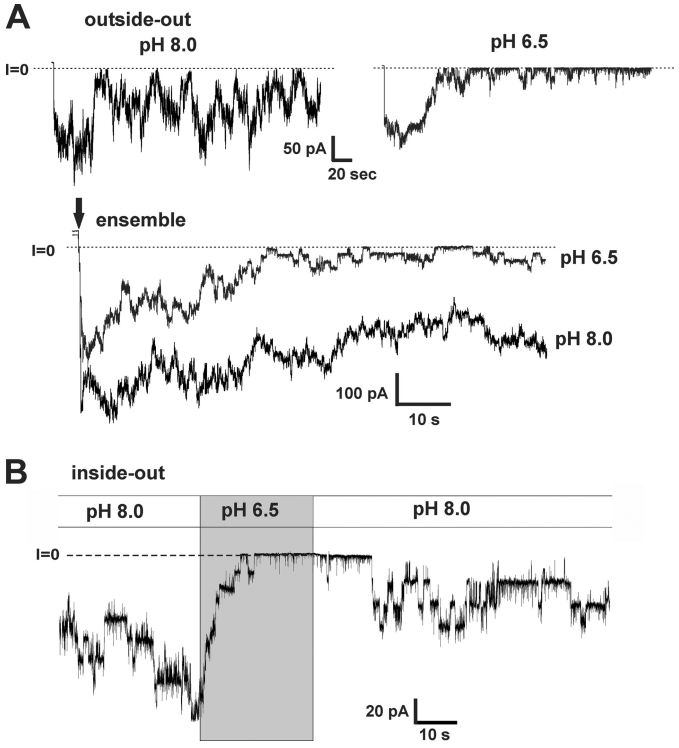

FIGURE 4. **pH is effective from either side of the membrane and promotes closure of the loop gate.** *A*, representative recordings of WT Cx26 hemichannels obtained from cell-attached patches. Patch pipettes were filled with IPS (see "Materials and Methods") and adjusted to pH 8.0 (*left trace*) or pH 6.5 (*right trace*). The bath was the same composition as the pipette solution, IPS buffered with HEPES, and was maintained at a pH of 8.0. Positive pressure to the patch pipette was released prior to making contact with the oocyte, allowing for brief mixing of bath and pipette solutions. Oocytes with high expression levels were used so that patches contained multiple hemichannels. Average current remained high throughout the recording (2–3 min) when the patch pipette was at pH 8.0 but quickly declined with pipettes filled with IPS at pH 6.5. Membrane voltage was stepped to −50 mV (at the *arrow*) to monitor the current over time. Shown are ensemble currents from multiple ($n = 7$) cell-attached patches for each pH using the same protocol. Currents declined rapidly using pipettes filled with IPS at pH 6.5. *B*, excised inside-out patch recording in symmetric IPS solution at pH 8.0 was briefly perfused with a pH 6.5 solution. Cx26 hemichannels closed in response to low pH and reopened upon washout.

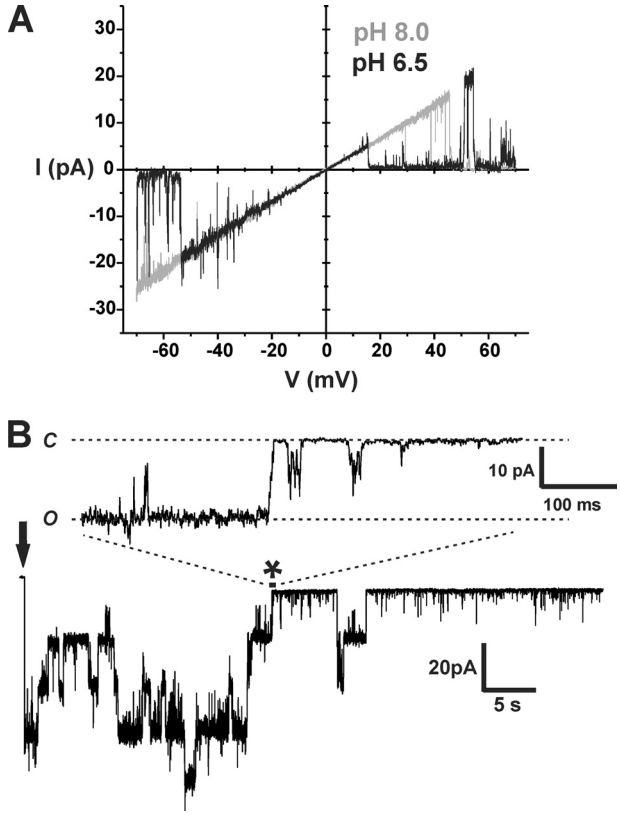

FIGURE 5. **Acidification does not affect unitary conductance but promotes closure of the loop gate.** *A*, superimposed cell-attached patch recordings containing single WT Cx26 hemichannels recorded using pipettes filled with IPS adjusted to pH 8.0 (*gray*) and IPS adjusted to pH 6.5 (*black*). Currents are in response to 8-s voltage ramps applied between +70 and −70 mV and leak-subtracted (see "Materials and Methods"). Unitary conductance was unaffected by pH. *B*, recording from a cell-attached patch containing ~4 hemichannels using a pipette filled with IPS at pH 6.5. The seal was obtained just prior to stepping the membrane voltage to −50 mV (*arrow*). Hemichannels closed in response to low pH. Expanded view of one of the closing events (*asterisk*) shows a transition consisting of several transient substates characteristic of loop gating. *C* and *O* refer to closed and open states, respectively.

was less sensitive, with inhibition shifted to higher concentrations. An excess of 10 μM Zn^{2+} was needed to achieve >50% inhibition in A40V. 100 μM Zn^{2+} produced nearly complete inhibition of WT and all three mutant hemichannels.

Pharmacological Studies of Hemichannel Modulation by pH and Zn^{2+}—As a first approach to assess whether His and/or Cys residues are involved in Cx26 hemichannel responses to pH and Zn^{2+}, we used pharmacology to try to narrow down candidate residues. We used DEPC, a His-modifying reagent (24), the MTS reagents MTSET and MTSEA, which specifically modify Cys residues (25), and NBS, a brominating and oxidizing reagent that preferentially oxidizes Trp residues in proteins and, to a lesser extent, in Tyr, His, and Met residues (26).

For pH, we applied pH 6.8 HEPES-buffered bath solutions to WT Cx26 (Fig. 7*A*) and A40V (Fig. 7*B*) hemichannels, which produced substantial reductions in current that readily reversed upon washout. Following treatment with MTSET (membrane-impermeant) or MTSEA (membrane-permeant), the responses to pH 6.8 were unaffected in either WT or A40V hemichannels. In contrast, treatment with NBS

FIGURE 3. **pH responses of WT Cx26 and A40V hemichannels are unaffected by pH buffers.** *A*, bar graph summarizing the effects of pH buffers on the pH responses of Cx26 WT and A40V hemichannels. In each buffer, currents were measured at pH 8.0 and pH 7.1 and plotted as the ratio *I*(pH 7.1)/*I*(pH 8.0). Oocytes were voltage-clamped and maintained at −40 mV. The *number* in each *bar* denotes the number of experiments in each buffer condition. *B*, examples of measurements of BCECF fluorescence in oocytes expressing WT Cx26 or A40V. Fluorescence (in arbitrary units, *A.U.*) was measured at 540 nm and plotted as the ratio obtained from 440- and 490-nm excitation wavelengths. Each *trace* represents fluorescence measured in a different region of interest. The regions of interest were randomly scattered throughout the cytoplasm of an oocyte. Exposure to the HEPES-buffered pH 6.8 solution for 2 min did not produce a measureable change in fluorescence, signifying no appreciable change in bulk cytoplasmic pH. However, exposure to the same pH (6.8) for 2 min in a bath solution buffered with $NaHCO_3$ produced a large fluorescence change indicative of substantial bulk cytoplasmic acidification. *C*, examples of recordings of hemichannel currents from the same oocytes as in *B*. For each series, oocytes were placed in 100 mM NaCl containing 10 mM HEPES adjusted to pH 8.0 and then exposed to pH 6.8 for several min. After returning to pH 8.0, the bath solution was switched to a pH 8.0 solution using 10 mM $NaHCO_3$ as a buffer and again exposed to the same pH (6.8) for several min. Oocytes were voltage-clamped and maintained at −40 mV throughout. The reductions in the hemichannel currents at pH 6.8 were essentially the same in both buffers, despite the large differences observed in bulk cytoplasmic acidification (see *B*). Extracellular Ca^{2+} was held constant at 0.2 mM. *Dashed horizontal lines*, zero membrane current levels ($I = 0$). *Error bars*, S.E.

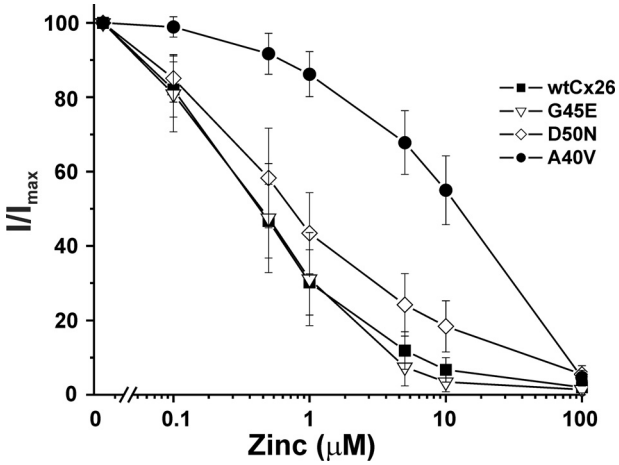

FIGURE 6. **A40V hemichannels are less sensitive to extracellular Zn^{2+}.** Summary of data for hemichannel inhibition by extracellular Zn^{2+} for WT Cx26 and three KID syndrome mutants, A40V, G45E, and D50N. Oocytes were placed in 100 mM NaCl containing 0.2 mM Ca^{2+} and 10 mM HEPES (pH 8.0) and sequentially exposed to the same solution with added $ZnCl_2$ in increasing concentrations ranging from 0.1 to 100 μM. At the end of each experiment, oocytes were returned to a solution with no added $ZnCl_2$. Oocytes were voltage-clamped and maintained at a constant voltage of −40 mV. Only data sets in which the currents remained fairly constant from the beginning to the end of the experiment were used. Data are plotted as the fraction of current remaining (I/I_{max}), with I_{max} the current measured with no added $ZnCl_2$. Data points represent mean ± S.D. (*error bars*); WT Cx26 ($n = 33$), A40V ($n = 27$), G45E ($n = 18$), and D50N ($n = 14$).

(250 μM) attenuated subsequent pH responses; NBS itself produced no appreciable effect on the hemichannel currents at this concentration. The degree of attenuation was greater for A40V, which was rendered poorly sensitive to pH 6.8. The same results were obtained whether or not MTS reagents were applied prior to NBS. Also of note, reversal upon washout following NBS treatment was incomplete for WT Cx26. A summary of results from a number of experiments compares the fraction of current remaining at low pH before and after NBS treatment (Fig. 7*C*). In each experiment, oocytes were returned to MND96 containing 1.8 mM Ca^{2+} to assess responsiveness to Ca^{2+} as a test of cell viability. Also, to test for thiol reagent activity, MTSET and MTSEA from the same stocks were applied to oocytes expressing Cys-substituted G45C hemichannels (Fig. 7*D*), which upon modification produce robust, rapid, and irreversible reductions in current due to altered charge in the pore as reported previously (5).

A parallel set of experiments examined effects on inhibition by Zn^{2+} (Fig. 8). Two concentrations of Zn^{2+} were examined, 10 and 30 μM. As for pH, responses to Zn^{2+} were unaffected by MTS reagents but were attenuated by NBS, particularly for the lower (10 μM) Zn^{2+} concentration; WT Cx26 was poorly inhibited, and A40V was rendered nearly insensitive. Again, as for pH, reversibility in WT Cx26 was incomplete following treatment with NBS. We could not examine higher concentrations of NBS (particularly >400 μM) because large leak currents developed in oocytes, both in Cx26-expressing and in control (water-injected) oocytes.

These correlative pharmacological data support the possibility that the residues mediating inhibition of Cx26 hemichannels by pH and Zn^{2+} overlap and that His residues may play a role. Unfortunately, we could not utilize DEPC, a more specific His-modifying reagent, because treatment with this reagent resulted in substantial and irreversible inhibition of Cx26 hemichannel currents (data not shown).

His Mutagenesis Studies—The crystal structure of the Cx26 GJ channel suggests that Ala-40 participates in an intrasubunit hydrophobic core centered around Trp-44 that stabilizes subunit (protomer) structure (18). An illustration of two subunits shows the arrangement of TM1 and TM2 transmembrane helices and a cross-sectional view of the aqueous pore (Fig. 9). The residues involved in the putative hydrophobic core are highlighted and include Trp-44, Ala-39, Ala-40, and Val-43 at the TM1/E1 border and Ile-74 in TM2. Also highlighted are the five His residues in Cx26 depicted with a *surface rendering* to illustrate putative solvent accessibility. Two of the His residues, His-67 and His-73, are in E1. His-67 is predicted to be readily accessible on the outer surface of the extracellular loops, whereas His-73 is deeper in the extracellular loop structure and in close proximity to Ala-40. His-100 is predicted to have exposure to the pore in the wide vestibule at the cytoplasmic end of the hemichannel, whereas His-16 and His-94 are predicted to be accessible from the cytoplasm.

In this study, we individually mutated these His residues to Asn or Ala residues and examined the effects on pH and Zn^{2+} responses. These substitutions resulted in functional hemichannels with the exception of H94A. For the two E1 residues, His-73 and His-67, substitutions resulted in pH sensitivities that were intermediate between WT and A40V (Fig. 10*A*). Zn^{2+} sensitivity was reduced only when His-73 was mutated and was intermediate between WT and A40V (Fig. 10*B*). For the two residues at the cytoplasmic end, His-16 and His-100, pH and Zn^{2+} sensitivities were reduced when His-16 was mutated; pH responses were similar to A40V, and Zn^{2+} was intermediate between WT and A40V. Mutation of His-100 essentially had no effect on pH or Zn^{2+} responses. All in all, these data indicate that no His residue stands out as a central determinant of pH and Zn^{2+} responses in Cx26 hemichannels. Thus, the effects of His substitutions probably represent more general structural effects, much like A40V. However, the differential effects of these His mutants on inhibition by pH and Zn^{2+} suggest that the underlying molecular components that mediate the responses to pH and Zn^{2+} are likely to differ.

DISCUSSION

In this study, we demonstrate that inhibition by pH and Zn^{2+} is altered in Cx26 hemichannels carrying the A40V KID syndrome mutation. In human skin, surface pH is substantially acidic, which helps maintain microbial balance and barrier homeostasis, but then follows a steep gradient toward plasma levels of ~7.4, moving to deeper layers of the epidermis, where connexins are expressed (27–30). In the cochlea, perilymphatic and endolymphatic compartments have pH values of 7.3 and 7.4, respectively (31). Thus, pH is likely to play a physiological role in limiting Cx26 hemichannel activity in these tissues. The reduced pH sensitivity for A40V we report here could nearly double hemichannel activity, comparable with that for reduced Ca^{2+} sensitivity previously reported for this mutant (5). Although we found sensitivity to extracellular Zn^{2+} reduced in

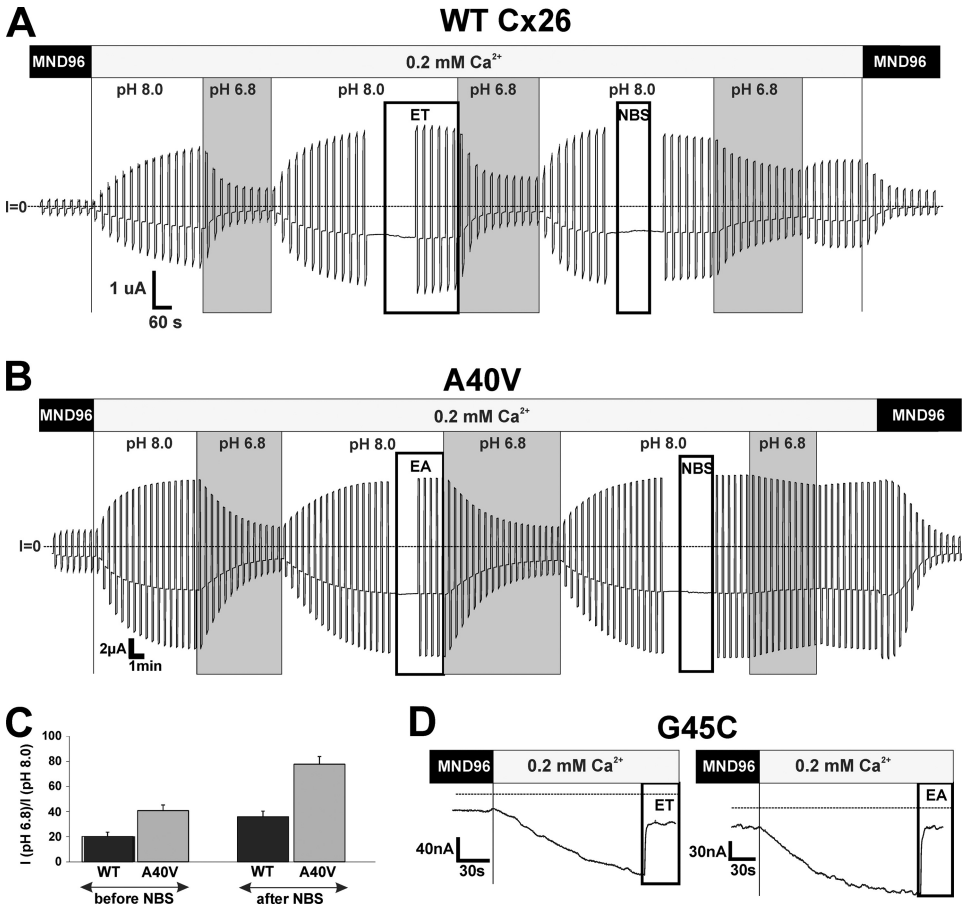

FIGURE 7. **NBS attenuates pH inhibition of Cx26 and A40V hemichannels.** Shown are representative recordings of Cx26 WT (*A*) and A40V (*B*) hemichannel currents illustrating pH responses before and after MTS and NBS treatments. Oocytes were clamped to −40 mV, and a voltage step protocol was applied repeatedly that consisted of a 5-s step to +50 mV followed by a 5-s step to −90 mV in 10-s intervals. MTS reagents (MTSET or MTSEA; 200 μM) and NBS (250 μM) were applied during the intervals indicated. Repeated voltage steps were briefly interrupted during drug perfusion to assess any rapid effects on hemichannel currents. Reponses to pH 6.8 were tested before and after each drug treatment. *Dotted horizontal lines*, zero membrane current ($I = 0$). MTS reagents had no effect on pH and Zn^{2+} responses. *C*, pH responses changed after treatment with NBS. Shown is a summary of results obtained at −40 mV. Results were the same for currents measured at +50 and −90 mV (data not shown). *D*, positive controls of reactivity of the same aliquots of MTS reagents in G45C mutants (see Ref. 5). *Error bars*, S.D.

A40V hemichannels, it is unknown whether free Zn^{2+} concentrations are in the range to play a role in cochlea and skin. Resting or tonic levels of free Zn^{2+} have been of particular interest in the nervous system, and measurements suggest a concentration in the 5–25 nM range, although vesicular release produces transiently higher concentrations (32). Of note, low serum zinc levels have been linked to various dermatological conditions (33).

Both pH and Zn^{2+} had been shown to inhibit Cx26 hemichannel currents expressed in *Xenopus* oocytes (17, 34). Our pH data are in general agreement with Ripps *et al.* (17), but for Zn^{2+}, we observed a higher sensitivity and a monophasic rather than a biphasic response, as reported by Chappell *et al.* (34). We have no explicit explanation for these differences, although the experimental protocols used by Chappell *et al.* (34) that stepped the membrane potential positive could progressively activate Cx26 hemichannels, which exhibit slow kinetics, thereby giving the appearance of a biphasic response with activation counteracting inhibition at low Zn^{2+} concentrations.

Examination of Cx26 at the single hemichannel level revealed several aspects of the effects of pH. First, acidic pH did not demonstrably alter the unitary conductance of the open state. Second, acidic pH induced full closures with gating transitions that resembled those characteristic of the intrinsic voltage-dependent loop gating mechanism (19). Last, using excised patches, we showed that pH was effective from either side of the membrane. Taken together, these results suggest that pH acts by protonating residues somewhere in the permeation pathway to bring about closure of the loop gate; there were no indications of novel, pore-blocking events, such as rapid or flickery closings. A similar conclusion was reached in studies of Cx46 hemichannels, and in addition, submillisecond solution switching showed no apparent delay in the onset of pH-induced closures indicative of a direct effect of H^+ on the hemichannel itself (15). Connexins differ from other voltage-dependent ion channels in that the voltage sensing elements are positioned such that they sense the local voltage in the pore (35–37). This design, unlike the separate voltage-sensing domains of K^+, Na^+, and Ca^{2+} channels (38, 39), allows GJ channels to sense the transjunctional voltage (*i.e.* the voltage difference between two cells, irrespective of the absolute values of the membrane voltages). Thus, there is a reasonable expectation for a link between protonation of pore residues and changes in voltage-dependent gating in connexin hemichannels.

The lack of an effect of pH on the unitary conductance of Cx26 hemichannels, despite the suggestion that protonation is

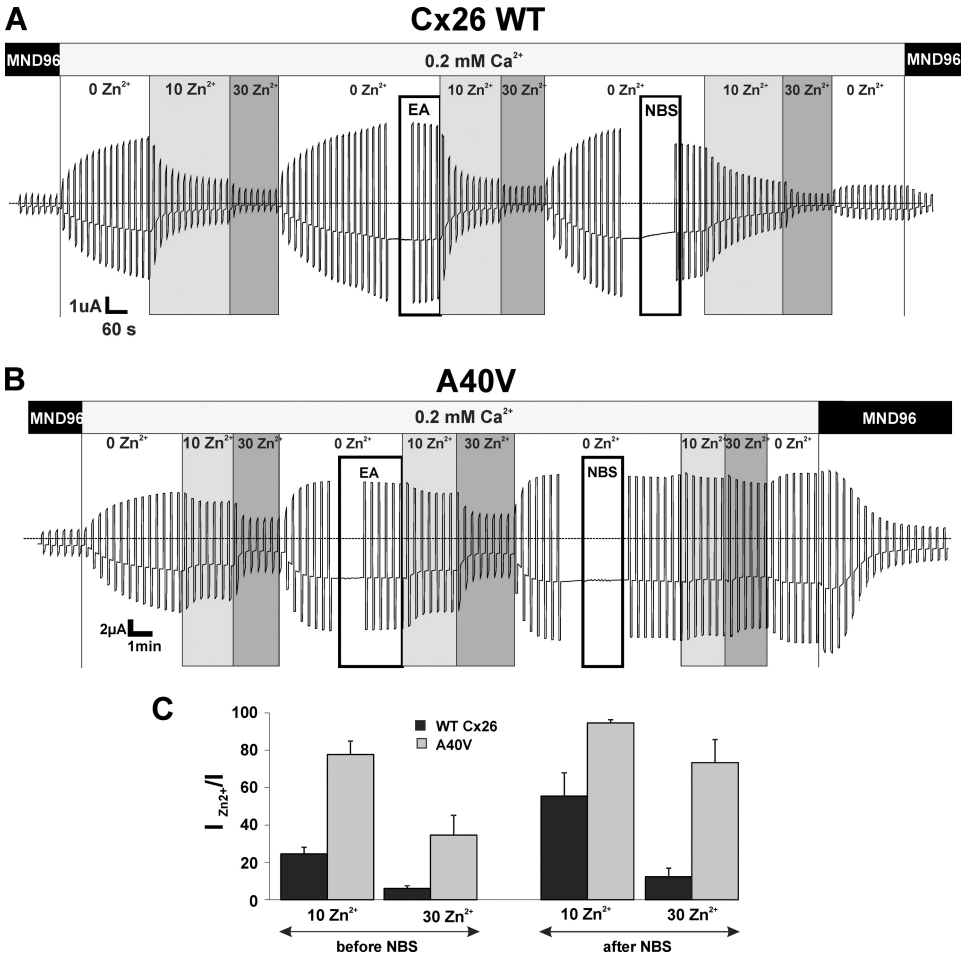

FIGURE 8. **NBS attenuates Zn^{2+} inhibition of Cx26 and A40V hemichannels.** Shown are representative recordings of Cx26 WT (*A*) and A40V (*B*) hemichannel currents illustrating Zn^{2+} responses before and after MTS and NBS treatments. The same repeated voltage step protocol was used as described in the legend to Fig. 7. Two Zn^{2+} concentrations were tested, 10 and 30 μM. *Dotted horizontal lines*, zero membrane current ($I = 0$). Positive controls for MTS reactivity (not shown) were similarly applied as described in the legend to Fig. 7. *C*, summary of results obtained at −40 mV. Results were the same at +50 and −90 mV (data not shown). *Error bars*, S.D.

occurring in the pore, could be explained if the protonated residues are in a wide region of the pore that is not rate-limiting for ion flux. A recent study of inhibition of Cx50 hemichannels by the charged quinine derivative *N*-benzylquininium showed no effect on unitary conductance despite evidence of binding in the pore (40). *N*-Benzylquininium was shown to promote closure of the loop gate, and chimeric analyses suggested a binding site in the NT domain, which contributes to the wide cytoplasmic vestibule of the pore. According to the crystal structure of Cx26, this region is ~40 Å in diameter, compared with ~14 Å in the narrow region of the pore funnel (18). Thus, a mechanism similar to that proposed for *N*-benzylquininium may occur with pH, with residues promoting closure of the loop gate upon protonation. Although His-100 was a good candidate residue for protonation in the pore, mutation of this residue had no effect of pH/Zn^{2+} sensitivities or gating.

pH sensitivity of Cx26-containing channels has been attributed to protonated forms of aminosulfonate pH buffers (21, 22). The closely related Cx32 isoform was found to be insensitive to aminosulfonates, indicative of a connexin-specific property. Recent studies in HeLa cells transfected with Cx26 using taurine, a biological amimosulfonate, suggested a mechanism for aminosulfonate sensitivity consisting of a pH-driven cytoplasmic interaction between CT and CL domains that is disrupted by aminosulfonates, thereby leading to closure (23). Inclusion of HEPES in the bath blocked the taurine transporter and, thus, taurine entry, thereby preventing pH-dependent closure of Cx26. We saw no differences in the magnitudes of the responses of Cx26 hemichannels to pH in *Xenopus* oocytes whether or not bath solutions included aminosulfonate buffers. In the case of Tris, we maintained oocytes in Tris buffer for several days to avoid loading cells with HEPES via Cx26 hemichannels or some other pathway. Moreover, the response of Cx26 hemichannels to acidification remained in excised, inside-out patches exposed to aminosulfonate-lacking buffers. We cannot exclude the possibility that endogenous ligands remain attached with patch excision that confer sensitivity to pH via a CL-CT interaction and/or that the cytoplasmic environments between oocytes and mammalian cells differ. Nonetheless, our data suggest that if a pH-driven interaction between cytoplasmic CT and CL domains is required for pH sensitivity, the relevant protonated residues are accessible to H^+ as it fluxes through the pore.

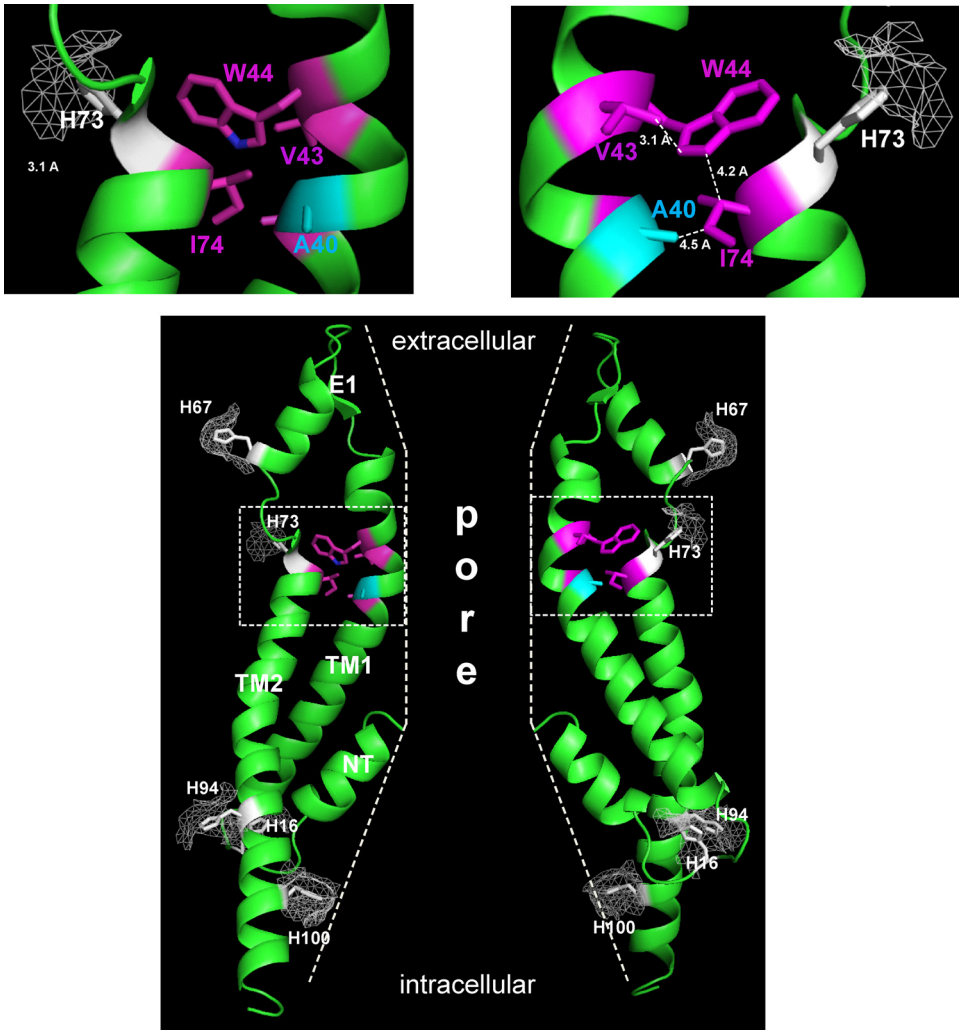

FIGURE 9. **A40V and intrasubunit interactions.** Shown is a representation of two of six subunits (*green ribbon*) around a central aqueous pore from the atomic structure of Cx26 (Protein Data Bank entry 2ZW3) (18). The side chain of Ala-40 (in *cyan*) is shown along with side chains of Ala-39, Val-43, Trp-44, and Ile-74 (in *purple*). These residues are proposed to participate in a hydrophobic core stabilizing intrasubunit structure. Side chains of all five His residues (*white*) are also depicted along with putative surface accessibility (*mesh*). *Insets* show *expanded views* of the *boxed regions* containing the hydrophobic core. The gross shape of the pore is illustrated by the *dashed lines*. *NT*, amino terminus; *TM1* and *TM2*, first and second transmembrane domains; *E1*, first extracellular loop domain. For better visualization of the hydrophobic core, the structure was truncated at residue Gly-109 at the cytoplasmic end of TM2. Structures are displayed using PyMOL software.

Along with A40V, we examined two other KID syndrome mutants, G45E and D50N, to assess whether deficiencies in regulation by pH and/or Zn^{2+} were common characteristics of KID mutants, particularly for those clustered near the border of TM1 and E1. However, impaired inhibition by pH and Zn^{2+} was limited to A40V. All three mutants show some degree of impaired inhibition by Ca^{2+} (5, 10, 11), but the magnitude of the effect ranged considerably from a small deficiency evident at positive potentials for G45E to a near loss of Ca^{2+} inhibition for D50N (14, 41). Thus, the molecular elements that mediate inhibition by Ca^{2+} and pH appear to be distinct, although it is possible they act on a common final pathway (*i.e.* the loop gating mechanism). Furthermore, D50N exhibits a similar sensitivity to Zn^{2+} as WT Cx26 despite lacking sensitivity to Ca^{2+}, suggesting that the molecular mechanisms leading to inhibition by Ca^{2+} and Zn^{2+} also differ. In the initial characterization of hemichannel currents in Cx46-expressing oocytes, inhibition by Ca^{2+} and other divalent cations were assumed to occur by the same mechanism with rank order potency Co^{2+}, $Ni^{2+} > Ca^{2+} > Mg^{2+}$ (42). In fish horizontal cells, the order of potency for hemichannel-mediated currents was reported to be $Zn^{2+} > Cd^{2+} > Co^{2+} > Ca^{2+} > Ba^{2+} > Mg^{2+}$, but Ca^{2+} and Zn^{2+} responses appeared to act independently (43). Horizontal cells express Cx57 in rodents, Cx50 in rabbits, and Cx55.5, Cx52.6, Cx52.7, and Cx52.9 in fish (44–47). Thus, the actions of divalent cations on hemichannels must be interpreted with caution because they may represent regulation by the same or different sites, depending on the divalent cation used and the connexin being examined.

The A40V mutation produces a multiplicity of altered biophysical properties that includes impaired inhibition by pH and Zn^{2+}, as we report here, as well as impaired inhibition by Ca^{2+} and slowed gating, as reported previously (5, 10). Such widespread effects suggest that the A40V mutation produces a sufficient perturbation in the structure of the Cx26 hemichannel that affects the properties of a residue(s) involved in these pro-

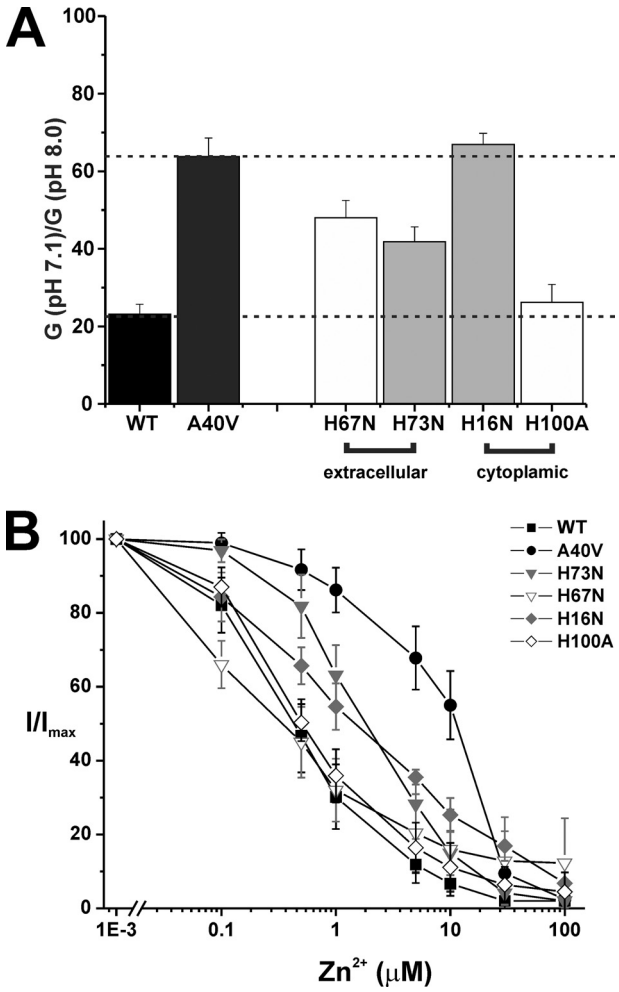

FIGURE 10. **Effects of His mutations in WT Cx26 on hemichannel pH and Zn^{2+} responses.** *A*, bar graph showing ratios of macroscopic conductances in pH 7.1 and 8.0 for Cx26 hemichannels containing single His mutations. Conductances were calculated from currents elicited by brief (500-ms) voltage steps of ±10 and ±20 mV applied from a holding potential of −20 mV. The calculated conductances were averaged for the ±10- and ±20-mV voltage steps; no voltage dependence was evident during these small, brief steps. *Dashed lines* highlight the values of the conductance rations for WT Cx26 and A40V hemichannels. Each *bar* represents the mean ratio ± S.E. (*error bars*). WT Cx26 ($n = 8$), A40V ($n = 5$), H67N ($n = 5$), H73N ($n = 6$), H16N ($n = 4$), and H100A ($n = 9$). *B*, summary of data for hemichannel inhibition by extracellular Zn^{2+} for the four His mutant hemichannels. Data for WT Cx26 and A40V are the same as in Fig. 6. Oocytes were placed in 100 mM NaCl containing 0.2 mM Ca^{2+} and 10 mM HEPES (pH 8.0) and sequentially exposed to the same solution with added $ZnCl_2$ in increasing concentrations ranging from 0.1 to 100 μM. At the end of each experiment, oocytes were returned to a solution with no added $ZnCl_2$. Oocytes were voltage-clamped and maintained at constant voltage of −40 mV. Data are plotted as the fraction of current remaining (I/I_{max}), with I_{max} the current measured with no added $ZnCl_2$. Data points are mean ± S.D.; WT Cx26 ($n = 33$), A40V ($n = 27$), H73N ($n = 10$), H67N ($n = 6$), H16N ($n = 7$), and H100A ($n = 5$).

cesses. The crystal structure of the CX26 GJ channel suggests that Ala-40 is part of a hydrophobic core that can function to stabilize subunit structure (18, 48). Thus, A40V probably perturbs the subunit structure in a way that either results in shifts in the pK_a values of relevant titratable residues as well as changes in the positions of residues involved in the coordination of Zn^{2+} or changes in the coupling of titration and Zn^{2+} coordination with hemichannel closure.

Although His and Cys residues are good candidates for mediating pH and Zn^{2+} responses, we saw no evidence for the involvement of Cys using thiol-modifying MTS reagents. The effects of NBS, however, suggest that His residues could be involved, although NBS is not specific for His, preferentially oxidizing Trp residues and, to a lesser extent, Tyr, His, and Met residues (26). NBS affected both pH and Zn^{2+} responses, appearing to shift their sensitivities. Moreover, the effect of NBS was more evident in A40V compared with WT Cx26. Following up with mutagenesis, individual mutation of any of the five His residues in Cx26 (His-16, His-67, His-73, His-94, or His-100) did not abolish pH or Zn^{2+} responses. His-94 was the only His that when mutated resulted in loss of hemichannel function. pH and Zn^{2+} responses were reduced for H73N, which is in E1 and in close proximity to the residues involved in the hydrophobic core (Fig. 9). H16N also reduced inhibition by pH and Zn^{2+}, whereas H67N modestly reduced pH responses, but showed no effect on inhibition by Zn^{2+}. H100A showed no appreciable effect on inhibition by pH or Zn^{2+}, although the crystal structure predicts exposure to the pore. The differential effects of these mutants on inhibition by pH and Zn^{2+} suggest that the residues mediating these two responses differ. More importantly, these data indicate that no individual His residue confers sensitivity to pH and Zn^{2+} in Cx26 hemichannels. Taken together, the effects we observed with mutations of His residues may not be specific to His protonation or to the binding of Zn^{2+} but rather due to effects similar to that of A40V, which is to perturb subunit structure, leading to impaired closure of the loop gate.

Interestingly, following NBS treatment and subsequent application of low pH or Zn^{2+}, WT Cx26 hemichannels did not recover fully upon washout. This phenomenon was not evident for A40V at the pH and Zn^{2+} concentrations used. However, if NBS-treated A40V hemichannels were closed by exposure to high (2.0 mM) Ca^{2+}, we observed the same phenomenon (*i.e.* little or no recovery upon returning to low Ca^{2+}) (data not shown). These data suggest that NBS may produce a state-dependent modification that blocks or markedly slows hemichannel reopening after closure. Closure can be by induced by Ca^{2+}, Zn^{2+}, or pH, consistent with the idea that these agents all promote closure of the loop gate.

In summary, excessive opening of Cx26 hemichannels is believed to underlie disease pathogenesis in KID syndrome. This study presents two new possible contributing factors, pH and Zn^{2+}. Both pH and Zn^{2+} are robust inhibitors of Cx26 hemichannels, with pH, in particular, effective in the neutral pH range and thus likely to play a physiological role. A40V shows a multiplicity of aberrant properties, suggesting that several mechanisms may combine to elicit pathology, with each alone, perhaps, insufficient or conferring mild phenotypes. These findings also demonstrate that differential sets of mechanisms contribute to hemichannel dysfunction in different KID syndrome mutants, which has important implications regarding genotype-phenotype associations and strategies for treatment. For patients carrying the A40V mutation, treatments containing zinc in topical ointments may be less effective in alleviating skin disorders.

REFERENCES

1. Lee, J. R., and White, T. W. (2009) Connexin-26 mutations in deafness and skin disease. *Expert Rev. Mol. Med.* **11,** e35
2. Levit, N. A., Mese, G., Basaly, M. G., and White, T. W. (2012) Pathological hemichannels associated with human Cx26 mutations causing Keratitis-

Ichthyosis-deafness syndrome. *Biochim. Biophys. Acta* **1818,** 2014–2019
3. Xu, J., and Nicholson, B. J. (2013) The role of connexins in ear and skin physiology: functional insights from disease-associated mutations. *Biochim. Biophys. Acta* **1828,** 167–178
4. Mese, G., Sellitto, C., Li, L., Wang, H. Z., Valiunas, V., Richard, G., Brink, P. R., and White, T. W. (2011) The Cx26-G45E mutation displays increased hemichannel activity in a mouse model of the lethal form of keratitis-ichthyosis-deafness syndrome. *Mol. Biol. Cell* **22,** 4776–4786
5. Sánchez, H. A., Mese, G., Srinivas, M., White, T. W., and Verselis, V. K. (2010) Differentially altered Ca^{2+} regulation and Ca^{2+} permeability in Cx26 hemichannels formed by the A40V and G45E mutations that cause keratitis ichthyosis deafness syndrome. *J. Gen. Physiol.* **136,** 47–62
6. Zhao, H. B., Yu, N., and Fleming, C. R. (2005) Gap junctional hemichannel-mediated ATP release and hearing controls in the inner ear. *Proc. Natl. Acad. Sci. U.S.A.* **102,** 18724–18729
7. Anselmi, F., Hernandez, V. H., Crispino, G., Seydel, A., Ortolano, S., Roper, S. D., Kessaris, N., Richardson, W., Rickheit, G., Filippov, M. A., Monyer, H., and Mammano, F. (2008) ATP release through connexin hemichannels and gap junction transfer of second messengers propagate Ca^{2+} signals across the inner ear. *Proc. Natl. Acad. Sci. U.S.A.* **105,** 18770–18775
8. Gossman, D. G., and Zhao, H. B. (2008) Hemichannel-mediated inositol 1,4,5-trisphosphate (IP3) release in the cochlea: a novel mechanism of IP3 intercellular signaling. *Cell Commun. Adhes.* **15,** 305–315
9. Stong, B. C., Chang, Q., Ahmad, S., and Lin, X. (2006) A novel mechanism for connexin 26 mutation linked deafness: cell death caused by leaky gap junction hemichannels. *Laryngoscope* **116,** 2205–2210
10. Gerido, D. A., DeRosa, A. M., Richard, G., and White, T. W. (2007) Aberrant hemichannel properties of Cx26 mutations causing skin disease and deafness. *Am. J. Physiol. Cell Physiol.* **293,** C337–C345
11. Lee, J. R., Derosa, A. M., and White, T. W. (2009) Connexin mutations causing skin disease and deafness increase hemichannel activity and cell death when expressed in *Xenopus* oocytes. *J. Invest. Dermatol.* **129,** 870–878
12. Terrinoni, A., Codispoti, A., Serra, V., Didona, B., Bruno, E., Nisticò, R., Giustizieri, M., Alessandrini, M., Campione, E., and Melino, G. (2010) Connexin 26 (GJB2) mutations, causing KID syndrome, are associated with cell death due to calcium gating deregulation. *Biochem. Biophys. Res. Commun.* **394,** 909–914
13. Mhaske, P. V., Levit, N. A., Li, L., Wang, H. Z., Lee, J. R., Shuja, Z., Brink, P. R., and White, T. W. (2013) The human Cx26-D50A and Cx26-A88V mutations causing keratitis-ichthyosis-deafness syndrome display increased hemichannel activity. *Am. J. Physiol. Cell Physiol.* **304,** C1150–C1158
14. Sanchez, H. A., Villone, K., Srinivas, M., and Verselis, V. K. (2013) The D50N mutation and syndromic deafness: altered Cx26 hemichannel properties caused by effects on the pore and intersubunit interactions. *J. Gen. Physiol.* **142,** 3–22
15. Trexler, E. B., Bukauskas, F. F., Bennett, M. V., Bargiello, T. A., and Verselis, V. K. (1999) Rapid and direct effects of pH on connexins revealed by the connexin46 hemichannel preparation. *J. Gen. Physiol.* **113,** 721–742
16. Beahm, D. L., and Hall, J. E. (2002) Hemichannel and junctional properties of connexin 50. *Biophys. J.* **82,** 2016–2031
17. Ripps, H., Qian, H., and Zakevicius, J. (2004) Properties of connexin26 hemichannels expressed in *Xenopus* oocytes. *Cell Mol. Neurobiol.* **24,** 647–665
18. Maeda, S., Nakagawa, S., Suga, M., Yamashita, E., Oshima, A., Fujiyoshi, Y., and Tsukihara, T. (2009) Structure of the connexin 26 gap junction channel at 3.5 Å resolution. *Nature* **458,** 597–602
19. Trexler, E. B., Bennett, M. V., Bargiello, T. A., and Verselis, V. K. (1996) Voltage gating and permeation in a gap junction hemichannel. *Proc. Natl. Acad. Sci. U.S.A.* **93,** 5836–5841
20. Trexler, E. B., Bukauskas, F. F., Kronengold, J., Bargiello, T. A., and Verselis, V. K. (2000) The first extracellular loop domain is a major determinant of charge selectivity in connexin46 channels. *Biophys. J.* **79,** 3036–3051
21. Bevans, C. G., and Harris, A. L. (1999) Regulation of connexin channels by pH. Direct action of the protonated form of taurine and other aminosulfonates. *J. Biol. Chem.* **274,** 3711–3719
22. Tao, L., and Harris, A. L. (2004) Biochemical requirements for inhibition of Connexin26-containing channels by natural and synthetic taurine analogs. *J. Biol. Chem.* **279,** 38544–38554
23. Locke, D., Kieken, F., Tao, L., Sorgen, P. L., and Harris, A. L. (2011) Mechanism for modulation of gating of connexin26-containing channels by taurine. *J. Gen. Physiol.* **138,** 321–339
24. Miles, E. W. (1977) Modification of histidyl residues in proteins by diethylpyrocarbonate. *Methods Enzymol.* **47,** 431–442
25. Karlin, A., and Akabas, M. H. (1998) Substituted-cysteine accessibility method. *Methods Enzymol.* **293,** 123–145
26. Spande, T. F., Witkop, B., Degani, Y., and Patchornik, A. (1970) Selective cleavage and modification of peptides and proteins. *Adv. Protein Chem.* **24,** 97–260
27. Lee, S. H., Jeong, S. K., and Ahn, S. K. (2006) An update of the defensive barrier function of skin. *Yonsei Med. J.* **47,** 293–306
28. Stefaniak, A. B., Plessis, J., John, S. M., Eloff, F., Agner, T., Chou, T. C., Nixon, R., Steiner, M. F., Kudla, I., and Linn Holness, D. (2013) International guidelines for the *in vivo* assessment of skin properties in non-clinical settings: part 1. pH. *Skin Res. Technol.* **19,** 59–68
29. Di, W. L., Rugg, E. L., Leigh, I. M., and Kelsell, D. P. (2001) Multiple epidermal connexins are expressed in different keratinocyte subpopulations including connexin 31. *J. Invest. Dermatol.* **117,** 958–964
30. Scott, C. A., Tattersall, D., O'Toole, E. A., and Kelsell, D. P. (2012) Connexins in epidermal homeostasis and skin disease. *Biochim. Biophys. Acta* **1818,** 1952–1961
31. Wangemann, P. (2006) Supporting sensory transduction: cochlear fluid homeostasis and the endocochlear potential. *J. Physiol.* **576,** 11–21
32. Frederickson, C. J., Giblin, L. J., Krezel, A., McAdoo, D. J., Mueller, R. N., Zeng, Y., Balaji, R. V., Masalha, R., Thompson, R. B., Fierke, C. A., Sarvey, J. M., de Valdenebro, M., Prough, D. S., and Zornow, M. H. (2006) Concentrations of extracellular free zinc (pZn)e in the central nervous system during simple anesthetization, ischemia and reperfusion. *Exp. Neurol.* **198,** 285–293
33. Kumar, P., Lal, N. R., Mondal, A. K., Mondal, A., Gharami, R. C., and Maiti, A. (2012) Zinc and skin: A brief summary. *Dermatol. Online J.* **18,** 1
34. Chappell, R. L., Qian, H., Zakevicius, J., and Ripps, H. (2004) Histidine suppresses zinc modulation of connexin hemichannels. *Biol. Bull.* **207,** 188–190
35. Spray, D. C., Harris, A. L., and Bennett, M. V. (1981) Equilibrium properties of a voltage-dependent junctional conductance. *J. Gen. Physiol.* **77,** 77–93
36. Harris, A. L., Spray, D. C., and Bennett, M. V. (1981) Kinetic properties of a voltage-dependent junctional conductance. *J. Gen. Physiol.* **77,** 95–117
37. Bukauskas, F. F., and Verselis, V. K. (2004) Gap junction channel gating. *Biochim. Biophys. Acta* **1662,** 42–60
38. Long, S. B., Campbell, E. B., and Mackinnon, R. (2005) Voltage sensor of Kv1.2: structural basis of electromechanical coupling. *Science* **309,** 903–908
39. Tombola, F., Pathak, M. M., and Isacoff, E. Y. (2006) How does voltage open an ion channel? *Annu. Rev. Cell Dev. Biol.* **22,** 23–52
40. Rubinos, C., Sánchez, H. A., Verselis, V. K., and Srinivas, M. (2012) Mechanism of inhibition of connexin channels by the quinine derivative *N*-benzylquininium. *J. Gen. Physiol.* **139,** 69–82
41. Lopez, W., Gonzalez, J., Liu, Y., Harris, A. L., and Contreras, J. E. (2013) Insights on the mechanisms of Ca^{2+} regulation of connexin26 hemichannels revealed by human pathogenic mutations (D50N/Y). *J. Gen. Physiol.* **142,** 23–35
42. Ebihara, L., and Steiner, E. (1993) Properties of a nonjunctional current expressed from a rat connexin46 cDNA in *Xenopus* oocytes. *J. Gen. Physiol.* **102,** 59–74
43. Sun, Z., Zhang, D. Q., and McMahon, D. G. (2009) Zinc modulation of hemi-gap-junction channel currents in retinal horizontal cells. *J. Neurophysiol.* **101,** 1774–1780
44. Dermietzel, R., Kremer, M., Paputsoglu, G., Stang, A., Skerrett, I. M., Gomes, D., Srinivas, M., Janssen-Bienhold, U., Weiler, R., Nicholson, B. J., Bruzzone, R., and Spray, D. C. (2000) Molecular and functional diversity of neural connexins in the retina. *J. Neurosci.* **20,** 8331–8343
45. Hombach, S., Janssen-Bienhold, U., Söhl, G., Schubert, T., Büssow, H.,

Ott, T., Weiler, R., and Willecke, K. (2004) Functional expression of connexin57 in horizontal cells of the mouse retina. *Eur. J. Neurosci.* **19,** 2633–2640

46. Zoidl, G., Bruzzone, R., Weickert, S., Kremer, M., Zoidl, C., Mitropoulou, G., Srinivas, M., Spray, D. C., and Dermietzel, R. (2004) Molecular cloning and functional expression of zfCx52.6: a novel connexin with hemichannel-forming properties expressed in horizontal cells of the zebrafish retina. *J. Biol. Chem.* **279,** 2913–2921
47. Klaassen, L. J., Fahrenfort, I., and Kamermans, M. (2012) Connexin hemichannel mediated ephaptic inhibition in the retina. *Brain Res.* **1487,** 25–38
48. Nakagawa, S., Maeda, S., and Tsukihara, T. (2010) Structural and functional studies of gap junction channels. *Curr. Opin. Struct. Biol.* **20,** 423–430